Masud-U RASHID[1]
Shuai GUO[1]
Tigist Fetene ADANE[1]
Cornel Mihai NICOLESCU[1*]

ADVANCED MULTI-FUNCTIONAL COATINGS
FOR VIBRATION CONTROL OF MACHINING

The paper present theoretical and experimental studies of the energy dissipation performance of a composite structure composed in a multilayer nano-composite damping coating applied on a tungsten carbide shim and placed beneath the cutting insert. The coated shim placed closed to the cutting zone is subjected to high compressive and shear stresses as well as high temperature. Therefore, apart from high damping capacity it requires high stiffness and high thermal resistance. The coated shim dissipates the high frequency oscillations produced at the tool-chip and tool-workpiece interfaces during the chip forming process. The use of coated shims demonstrates that the tool life is considerably extended, while the machined surface integrity is improved. The Reuss model of the composite structure composed of a phase with a stiff, low loss factor and a phase with high loss factor is used to calculate the optimal coating thickness that gives high loss factor combined with high stiffness. The synthesis process of the coating material using HiPIMS process is discussed. The physical characteristics of the coating and the machining performance are presented in the experimental section.

1. INTRODUCTION

The competitiveness of manufacturing companies within industrial areas relies on efficient, flexible, and high-quality manufacturing processes. In turn, the efficiency and stability of manufacturing processes depends critically on the performance of the cutting tools employed. Two of the most important characteristics that affect manufacturing performance are surface integrity of machined parts and tool life. The first feature is related to the part design specification while the second is related to manufacturing process performance. In many instances, the main cause of deterioration of surface finish and tool life originates from a common source, i.e. vibration.

Vibrations and shocks next to the heat are the main causes for the failure or/and excessive wear of cutting tools, deterioration of surface finish and they significantly contribute to the rework and scrap, and consequently to poor quality.

_____

[1] Department of Production Engineering, KTH-Royal Institute of Technology, Stockholm, Sweden
[*] E-mail: gmni@kth.se

The total cost of repair, rework, scrap, service calls, warranty claims and write-offs from obsolete finished goods, called cost of poor quality (COPQ), amounted to 20 percent of the annual sales for manufacturing companies. A 20 percent COPQ implied that during one day of each five-day workweek, the entire company spent time and effort making scrap, which represented a loss of approximately €20,000 per day for a company with annual sales of €25 million. Experts have estimated that COPQ typically amounts to 5–30 percent of gross sales for manufacturing and service companies. Independent studies reveal that COPQ is costing companies millions of Euros each year, and its reduction can transform marginally successful companies into profitable ones [1].

Vibration occurs naturally during the cutting process and cannot be avoided. Material failures due to vibrations are unpredictable and cause damage not only to the tool, and to the final product, but also to the structural elements of the machine tool.

Keeping tool wear rate low sustains process dependability; while maintaining the process stability favours low vibration levels that prolong tool life and keeps the surface finish within required range. Both these actions result in high productivity and quality of the parts. Cutting tools get degraded by wear, which leads to a poor quality of parts and a significant increase of costs due to the need of post-processing and re-work. Premature worn tools increase the rejects and scrap and decreases the productivity due to rework and low product quality. Failing to change the tool in time results in breakage of the tool with disastrous consequences for the tool holder system, workpiece and/or machine tool structural components. Failures are frequent and result therefore in a significant downtime of production lines, and in lower production quality and volumes.

Vibration damping is a key issue in high-precision machining where vibrations have to be kept at a minimum level. Fatigue life of cutting tools can be also extended by increasing the vibration damping.

The purpose of this paper is to present a method for improving the cutting process efficiency and the integrity of the machined parts by controlling the vibration at the cutting tool edge. For this, the dynamic machining system is considered in stable state, i.e., the system is not exposed to self-excited vibrations or resonance related with heavy vibration generated by forced dynamic loads. In these stable conditions, the damping mechanism is applied close to the source of vibration, i.e., at the cutting insert. The benefit of this approach is that the high frequency parasite vibrations generated by the cutting force are suppressed, which results in reducing the wear rate, improved machined surface integrity and better process stability. In most of the research studies on machining system vibration, the main objective is suppression of self-excited-vibration or chatter. The current methods, based on passive damping in metal cutting, use TMD systems placed inside the tool holder. As these systems are tuned on a single natural frequency i.e., the tool holder natural frequency, they have limited effect in the wide range of excitation frequencies. There are other methods, with limited applications in metal cutting, making use of sensors and actuators to attain vibration sensing and activation to suppress the vibration in real time [2].

Currently no general vibration-damping solution is implemented in machining. A few alternative solutions for specific application do exist, but all suffer from severe limitations. The existing commercial solutions target primarily damping of unstable vibration (chatter) and are only efficient in the low frequency range. They are preventing heavy vibration

especially of tools with high ratio length-to-diameter. Vibration damping technologies are available only for a few very specific applications, such as tuned mass dampers for large diameter (>10 mm) toolholders. Silent Tools™ is a family of toolholders for turning, milling, boring and drilling. With a TMD mechanism in the tool body, the toolholders are specially designed to minimize vibration for long overhang [3] Overall, the general problem remains still unsolved.

In order to suppress vibrations close to the cutting edge, special materials have to be developed. These materials must resist higher mechanical and thermal loads, which characterizes the cutting zone.

This paper presents the development and investigation of the performance of advanced multi-functional nano-coatings coatings in cutting applications. Taking into consideration the location of the coating close to the cutting zone Fig. 1, the coating has to be endowed with specific mechanical, thermal and tribological features.
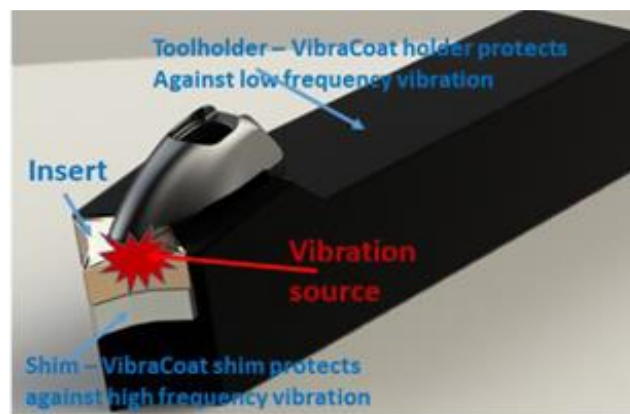

Fig. 1. Coated shim placed beneath the cutting insert

The coated material is applied on shims located under the cutting insert. For conventional tools, the shim protects the toolholder for damage in case the insert brakes down. In the present case, new functions have been added to the coated shims: high stiffness at elevated temperatures to resist high-level compressive stress, damping capacity to dissipate vibration produced by chip formation and good hardness and toughness to withstand mechanical and thermal loads.

Coatings can be employed to increase the global dissipative properties of a mechanical component with limited influence on the other mechanical properties. Mechanical components with high stiffness, thermal resistance and vibration damping specifications are in great demand for most mechanical engineering applications [4] The coated component dissipative properties can be significantly tailored by means of the application of coating layers with high internal hysteresis or with high frictional actions at the interface between the different layers.

Friction and vibration interact with each other in a dynamical system with sliding interface. Friction- induced vibrations are generally time- varying, nonlinear and stochastic. Though tribology and mechanical vibration used to be two distinct fields with the recent rapid

developments in the area of friction–vibration interactions, engineers are starting to combine tribology and mechanical vibrations as efficient methods to solve problems in engineering applications.

Understanding the tribological conditions at the tool-chip and tool–workpiece interfaces contributes to improving the cutting efficiency by the reduction of tool premature failures. The friction phenomena at these two interface zones usually give rise to vibrations, which propagate into the surrounding structural elements. Vibrations also affect interface friction, as friction and vibrations interact with each other. On the tool-chip interface, the contact load is concentrated on a very small area and, as a result, very high normal and shear stresses acting on the interface with maximum values of $\sigma_c = (900–1600)$ MPa and τ_c of about $(30–60\%)$ σ_c are documented [5].

From the tribo-mechanical system viewpoint, the chip formation mechanism is a cyclic process. As a result, vibration is generated due to friction conditions at the tool–chip and tool–workpiece interfaces and b chip segmentation. Plastic deformation of the chip in the secondary deformation zone (SDZ) is performed under upper boundary conditions with an additional influence of high temperatures. As the normal force increases, the contact area increases, and the peaks are flattened. Asperity junctions grow until they can support the applied load. Adhesive bonds form at the contact points. When a tangential force is applied, the bonds are broken, and overcoming the shear strength of the bonds results in the friction force [6] By forming and breaking adhesive bonds vibration is caused.

2. VIBRATION DAMPING

The vibration damping effect for a dynamic system is achieved by converting mechanical energy of the vibratory motion into other types of energy, most frequently heat, which can be evacuated from the system, [7] The damping capacity ψ is defined as the ratio of the energy that is dissipated per cycle to the total energy present in the vibrating system. The loss factor η is defined similarly as the ratio of the energy that is dissipated per radian to the total energy. If D denotes the energy dissipated per cycle and W the total energy in the system, then the loss factor is [7].

$$\eta = \frac{\psi}{2\pi} = \frac{D}{2\pi W} \tag{1}$$

In a dynamic system with viscous damping, the energy dissipated corresponds to the work that is done on the dashpot, that is the energy dissipated per cycle in a steady vibration at radian frequency ω and displacement amplitude X

$$D = \pi \omega_c X^2 \tag{2}$$

The total energy W stored by the system consists of the kinetic energy W_{kin} of the mass and the potential (or strain) energy W_{pot} in the spring

$$W = W_{kin} + W_{pot} \tag{3}$$

2.1. DAMPING MECHANISMS

Damping mechanisms involves mechanisms that convert mechanical energy into heat, as well as others that transport energy away from the vibrating system [7].

Lazan [8] classifies damping into two major types: material damping and system damping. According to Lazan, the material damping includes mechanisms of internal friction, internal damping, and hysteretic damping, which are related to the energy dissipation in a volume of macro-continuous media. The term macro-continuous is intended to exclude the damping in a configuration originating at interfaces between recognizable parts. Accordingly, material damping is associated with the energy dissipation which takes place when a homogeneous volume is subjected to cyclic stress and the damping mechanisms are associated with the internal microstructure of the material.

In system damping, energy is dissipated in various types of joints, interfaces, or fasteners. Interface slip has the capacity of dissipating large amount of energy. While material damping in a structure depends on its material composition and constitution as well as on stress amplitude, slip damping at an interface depends on another set of parameters, which include the coefficient of friction, pressure, shear stress, and strain distribution. Furthermore, material damping occurs throughout the volume of a part (a volume integral), whereas slip damping occurs at an interface surface only (a surface integral) [8]. The damping into joints in many complex mechanical structures is dominant compared to the usually very low damping of the metallic material itself. Local joints can effectively contribute to the damping behaviour of the whole structure. Friction, which dissipates energy during the vibration of a structure, is always present in mechanical joints. The vibrational damping occurs when small relative movements take place between the joint interfaces [9].

Damping of a vibrating structure may also result from friction associated with relative motion between the structure and solids or fluids that are in contact with it. Also, an electrically conductive structure moving in a magnetic field is subject to damping due to eddy currents that result from the motion and that are converted into heat [2].

2.2. DESIGNED-IN DAMPING METHODS

Passive damping may be broken into two classes: inherent and designed in. Inherent damping is damping that exist in a structure due damping mechanism described above. The level of inherent damping in a structure is usually less than 2 percent structural. Designed-in damping refers to passive damping that is added to a structure by design. This damping supplements inherent damping and it can increase considerable the passive damping of a structure [10].

Designed-in damping of a structure can be achieved by passive or active methods. Passive methods employ the inherent ability of certain materials to absorb the vibrational energy (for example, through mechanical deformation), thereby providing passive energy dissipation. Active methods make use of sensors and actuators to attain vibration sensing and activation to suppress the vibration in real time [2].

According to Johnson [9], approximately 85 percent of the passive damping treatments in actual applications are based on viscoelastic materials.

Design-in passive damping methods may include damping layers applied over large areas or discrete dampers attached to the structural system components [11]. Layer treatments usually rely upon material damping mechanisms [12] whereas common types of discrete damping treatments include dynamic absorbers, dashpots, inertial, friction, tuned, and broadband viscoelastic dampers.

Viscoelastic materials (VEMs) are widely used as damping layers for passive damping in industrial application. Viscoelastic materials are elastomeric materials whose long chain molecules cause them to convert mechanical energy into heat when they are deformed [10]. A detailed presentation of viscoelastic materials can be found in Ferry [13]. The *f* VEM passive damping methods depends on frequency and temperature.

Discrete dampers can be very effective and may be easy to design and implement. Tuned mass dampers (TMD) are commonly used in mechanical structures. A TMD is a discrete damping device attached to the structure at or near to an antinode or mode of vibration. These devices transfer energy at a resonance to two new system resonances each highly damped. TMDs are in general very efficient for single mode damping.

2.3. DAMPING OF CUTTING TOOL VIBRATIONS

Vibration damping can be a key issue in high-precision machining where vibrations have to be kept at a minimum level. Also, fatigue life of cutting tools can be extended by increasing the vibration damping.

For structural components that may be considered as uniform plates, one may estimate the loss factor η_b associated with energy loss at the plate boundaries, due to both energy transport to adjacent plate and dissipation at its boundaries, from information on the boundary absorption coefficients. For a plate of area, A, vibrating at a frequency at which the flexural wavelength λ on the plate is considerably shorter than a panel edge, this loss factor is given by

$$\eta_{\mathrm{b}} = \frac{\lambda}{\pi^2 A} \sum \gamma_i \, L_i \tag{4}$$

where γ_i denotes the absorption coefficient of the ith boundary increment whose length is L_i and where the summation extends over all boundary increments. At frequency f, the flexural wavelength on a homogeneous plate of thickness h of a material with longitudinal wave speed c_{L} and Poisson's ratio v is given by

$$\lambda = \sqrt{(\pi/\sqrt{3})h c_{\mathrm{L}}/f(1 - v^2)} \tag{5}$$

The absorption coefficient γ of a boundary element is defined as the fraction of the plate bending-wave energy impacting the boundary element that is not returned to the plate.

The energy that coated shims attached to the insert can dissipate, and thus the damping they can produce, depends markedly on the fastening method used. Coated shims attached to

WC inserts in such plates generally produce little damping if they are joined by means of a rigid adhesive. However, they can contribute significant damping if they have a free contact. At high frequencies, at which the flexural wavelength on the insert is smaller than the thickness of the coated shim, damping results predominantly from interface friction, coating layer friction and from the shear strain variation produced on the coating volume. The insert connected to the coated shim is damped not only due to energy dissipation within the shim but also due to energy transport to adjacent tool holder.

If a structural element is attached to a vibrating structure at a given point, then the energy D that is transported to the attached structure per cycle at frequency f is given by [14].

$$D = \frac{V_S^2 \, Re[Z_A]}{2f} \left| 1 + \frac{Z_A}{Z_S} \right|^{-2}$$
(6)

Here V_S denotes the amplitude of the velocity of the vibrating structure at the attachment point before the added structure is attached; Z_A denotes the driving point impedance of the attached structure, and Z_S denotes the impedance of the vibrating structure at the attachment point (with both impedances measured in the direction of V_S). The loss factor contribution due to an attached structure may be found by use of Eq.(1).

3. COATING THICKNESS CALCULATION

The coated shim placed beneath the insert, apart from the ability to damp mechanical vibrations, must be also endowed with relatively high stiffness and heat resistance. The shim is made of WC + Co, tungsten carbide and cobalt, by the same technology as cutting inserts. Tungsten carbide is approximately twice as stiff steel, with a Young's modulus of approximately 530–700 Gpa, and is double the density of steel. The strength of a material is characterized by complex modulus E^* under vibration conditions:

$$E^* = E' + jE''$$
(7)

in which E', E'' are storage modulus, loss modulus, respectively; and the module of E^* is detonated as $E = \sqrt{E'^2 + E''^2}$ and the loss factor $\tan \delta$ is a measure of damping and is expressed as the ratio of the imaginary part to the real part of the complex modulus E^*

$$\tan \delta = \frac{E''}{E'}$$
(8)

Since elastic modulus E measure the stiffness of the materials and $\tan \delta$ the damping, the product $E^* \tan \delta$ is a useful performance indicator that can be used for designing coatings with optimal properties.

The method used in this paper to calculate the product $E^* \tan \delta$ is based on Reuss model. The coated shim can be regarded as a composite structure with two phases, the coating and the substrate. According to Reuss model, when the load is applied perpendicular to the composite structure, the complex modulus of the composite structure is:

$$\frac{1}{E^*} = \frac{h_S}{E_S^*} + \frac{h_C}{E_C^*} \tag{9}$$

where h_s and h_c are the thickness of the substrate and of the coating respectively. By replacing the complex modulus with $E^* = E' + jE''$ and separating the real and complex parts, expressions for the elastic modulus, E, and loss factor, $\tan \delta$, are obtained for the composite structure as functions of the ratio E_c/E_s and the thickness ratio h_c/h_s.

Assuming the elastic stiffness, E_s of the substrate equal to 630 GPa, the loss factor of the substrate, $\tan d_s$ equal to 0.001, and the loss factor of the coating, $\tan \delta_c$ equal to 0.12, the optimal coating thickness can be determined with respect to the stiffness of the coating structure (Fig. 2). For E_c/E_s ratio (E_s = 630 MPa) equal to 0.2, the optimal thickness is h_c = 19% of the total composite structure (Fig. 3). As the coating stiffness decreases the participation of the coating to the whole structure size increase. For a coating stiffness equal to 126 GPa, the coating thickness has to reach 60% of the total thickness of the structure (Fig. 4).
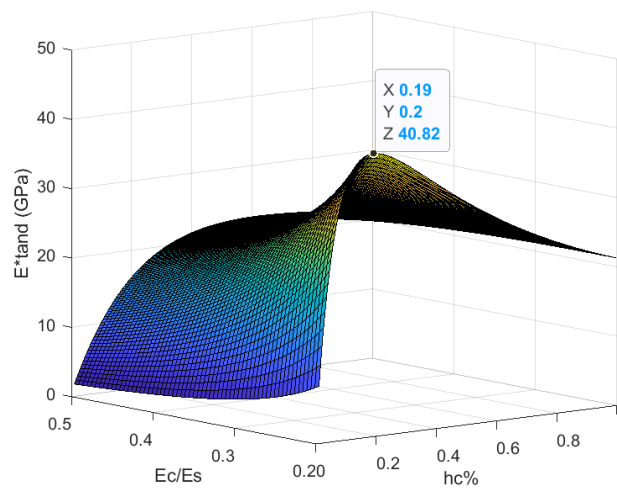
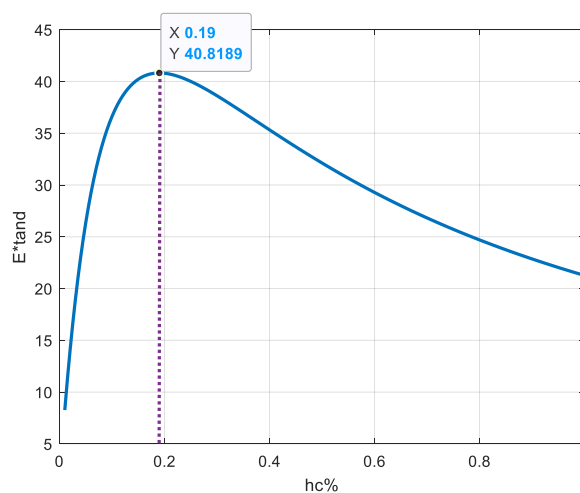Fig. 2. $E^*\tan \delta$ function for $E_c/E_s = 0.2$, $\tan \delta_s = 0.001$ and $\tan \delta_c = 0.12$

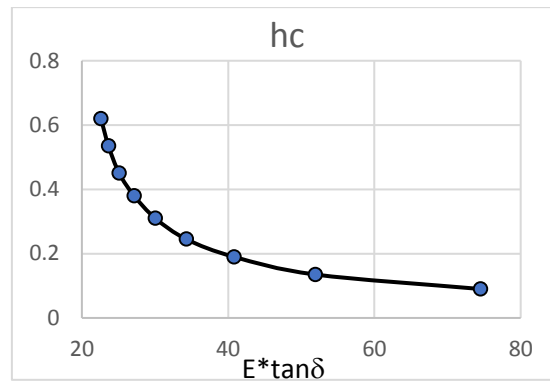Fig. 3. Calculation of the optimal coating thickness from the diagram h_c as a function of $E^*\tan \delta$

Fig. 4. Variation of the coating thickness, h_c, as a function of $E^*\tan\delta$

4. EXPERIMENTAL STUDY

4.1. SYNTHESIS OF NANO-COMPOSITE MULTILAYER CU:CUCN$_X$ COATING MATERIAL

Cu:CuCN$_x$ multilayer nano-composite damping coating material was synthesized by double cathode High Power Impulse Magnetron Sputtering (HiPIMS) deposition process coupled with Plasma Enhanced Chemical Vapor (PECVD) system shown in Fig. 5. The details of such a system is described elsewhere [15, 16]. The double cathode deposition chamber used in this work is cylindrical in shape, height 67 cm and diameter 63 cm, and equipped with three HiPIMS power source systems (IMPULSE™ 2-2, Starfire) powered by three DC power supply (PD500X, KJLC). Two of the HiPIMS units were connected to two cathodes and one unit was connected to substrate holder in master-slave configuration. For plasma etching process, the substrate holder was connected with medium frequency AC power supply (HV-AC-350K, Foton) capable of delivering 1200 V at 350 kHz. One copper (Cu) target (purity 99.99%) and one Ti target (purity 99.99%) of dimension length×width: 27.5 cm×10 cm were used for this deposition process. Cu atoms were sputtered in reactive nitrogen (N_2) and acetylene (C_2H_2) gaseous environment mixed with argon (Ar) gas, and in this way the plasma created in this HiPIMS process can be characterized as a highly dense one which can be an order of 10^{18} m^{-3} [17]. The sputtered metal atom become ionized due to high energy collisions among the electrons and gaseous (Ar, N_2 and C_2H_2) ions, molecules and energetic radicals, and consequently composite material species are formed and deposited on the substrates [18].

The substrate holder was placed 10 cm away from each target and kept rotating at 2 rpm during the whole deposition process so that homogeneous coating with lower internal residual stress is deposited onto the shims (Fig. 5b) [19]. Comparing to traditional PVD process one of the main advantages of HiPIMS system is that magnetron sputtering can be operated in lower process pressure [19]. The unbalanced-closed magnetic field between two cathodes, used in this study, as well as the electric field across the plasma guides and manipulates the highly ionized deposition flux towards the substrate. It has been demonstrated by several studies that the total energy flux towards the substrate in the HiPIMS discharge is mainly composed of ions [20, 21].
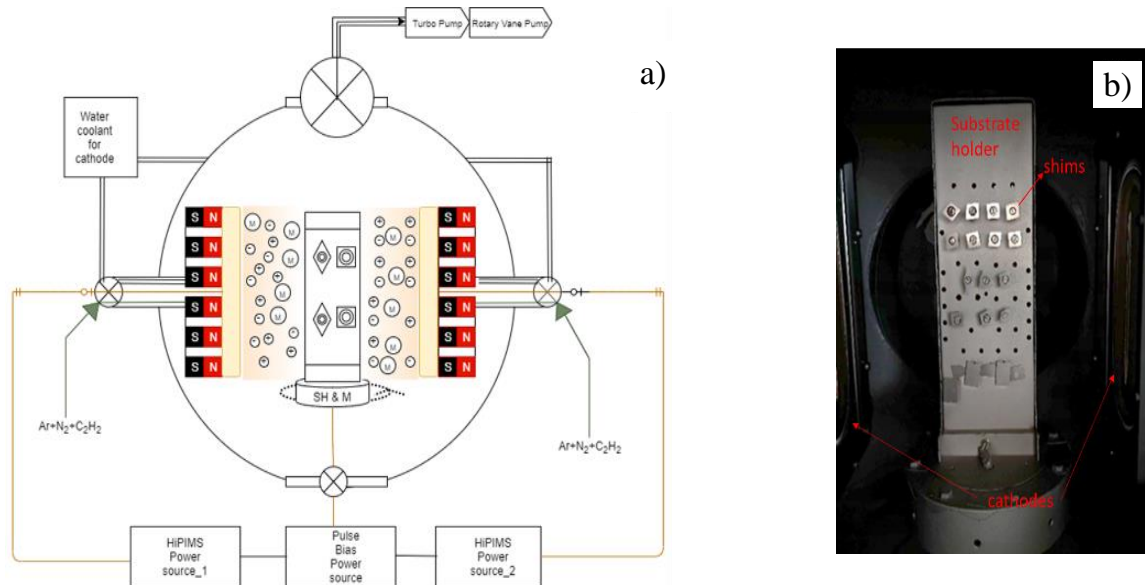
Fig. 5. a) Double cathode reactive HiPIMS shematic diagram, b) Inside of the HiPIMS deposition system

Prior to the deposition process the vacuum chamber was pumped down to the background pressure of 0.03 Pa. The substrate samples (shims and steel discs for material characterization) were mechanically and chemically cleaned. Details of this procedure is described in [22] Before starting the multilayer coating synthesis process, in-situ high pressure Ar gas plasma cleaning as well as low pressure HiPIMS metal ion plasma cleaning of the substrate were done. The multilayer coating was deposited at ambient temperature and no external heat was applied to the substrate. The details of process parameter can be found in Table1. During the deposition of both Cu and $CuCN_x$ layers, at the end of main pulse after 10 μs a positive reverse pulse of 100 V for 20 μs duration was applied to the cathode.

Table 1. Process parameters for depositing $Cu:CuCN_x$ coating in reactive-HiPIMS deposition process

Coating composition	Process time	Gas composition	Process Pressure (Pa)	Peak discharge Power Density (kW/cm²)	Duty Cycle (%)	Sync Bias Voltage (V)	Sync. Bias pulse frequency (Hz)	Pulse Bias duration (μs)
Ar^+ plasma ecthing	5 hr	Ar = 42 sccm	14.27	-	-	−600	3.50E+05	-
Ti^+ /Ar^+ plasma etching	2 hr	Ar = 42 sccm	1.1	0.27	-	−800	3.50E+05	-
Pre Ti layer (0.18 μm thick)	30 min	Ar = 14 sccm	0.4	0.42	1	−500	3.50E+05	-
$CuCN_x$ thick layer		Ar:N2:C2H2 = 14:10:10 sccm	0.72	0.63	1.05	−60	150	100
Cu interlayer	97 hrs	Ar = 14 sccm	0.42	0.55	1.4	−60	150	100
$CuCN_x$ thin layer		Ar:N2:C2H2 = 14:10:10 sccm	0.71	0.63	1.05	−60	150	100

4.2. MULTILAYER COMPOSITE COATING MATERIAL CHARACTERIZATION

The microstructure of multilayer nano-composite coating was studied by a Field Emission Scanning Electron Microscope (FESEM JEOL JSM-7001F) using an inLens detector. For cross-section imaging, coated small steel disk samples were mounted in an epoxy resin followed by mechanical polishing (from coarser sandpapers to final polish with diamond and silica nanoparticles). Elemental composition of different layers of the coating material were analyzed by the in-situ Energy-dispersive X-ray spectroscopy (EDS) analyzer equipped with with Si(Li) crystal detector. For elemental composition X-ray were collected from 3 different areas of each $CuCN_x$ and Cu layer.

Density of the coating material was determined by dividing the measured weight difference of a Ø12 mm steel disc (before and after being coated) with the volume of the coating. Surface and cross-sectional micro hardness of the coating material were determined by the Vickers micro hardness instrument (Qness Automatic Micro Hardness tester). For surface micro-hardness, maximum applied load was 10 N and holding time was 10 s at the maximum indentation depth (20 ± 2 µm). For cross-sectional micro hardness measurement, maximum applied load force was 0.25 N, and holding time was same at the maximum indentation depth of 2 ± 0.3 µm. Total 5 and 4 indents were performed respectively for surface and cross- sectional micro hardness measurement.

The friction coefficient (COF) of the coating material was measured as well as the adhesion critical load of the coating material was estimated by a scratch tester equipment (ForceBoard™ – Scratch and linear wear testing, Sweden). For scratch testing a HRC-3 Rockwell diamond probe of 200 µm tip radius was used.

4.3. MACHINING TEST SETUP

Continuous longitudinal external turning operation was performed using conventional (uncoated) and coated tungsten carbide shims to investigate the effect of $Cu:CuCN_x$ multilayer nano-composite coating on cutting tool life. The turning operation was conducted in SMT-Swedturn-ST300 CNC turning machine with coolant (Fig. 6a). The workpiece material was SS2541-03 alloy steel (34CrNiMoS6) with a diameter and length of 122 mm and 550 mm respectively and hardness of 290 HB. Several tests were conducted under stable turning conditions for 32 minutes each. For each test MIRCONA cutting inserts (MIRCONA SNMG 120408-NM7) with nose radius 0.8 mm and rake angle 75°C in MIRCONA tool holder (MIRCONA MSRNR 2525-12) were used. For each test same recommended cutting parameters, from cutting insert manufacturer, were used such as surface speed S 200 mm/min, feed rate f 0.4 mm/rev and depth of cut a_p 1.2 mm.

An ultra-miniature accelerometer (DYTRAN 3224A1) with a sensitivity of 11.20 mV/g was mounted on tool holder to acquire the acceleration signals in tangential direction (perpendicular to cutting direction) during the machining test (Fig. 6b). The clamping torque of cutting tools was kept the same during the tests with conventional and coated shims and the accelerometer was on the back side of tool holder, placed as close as possible to the cutting

zone (Fig. 6b). This kind of arrangement of the accelerometer is suitable for capturing very high frequency vibration of the cutting process. For each cutting run vibration signals (acceleration) were analyzed by LMS Test.Lab system connected to the accelerometer.
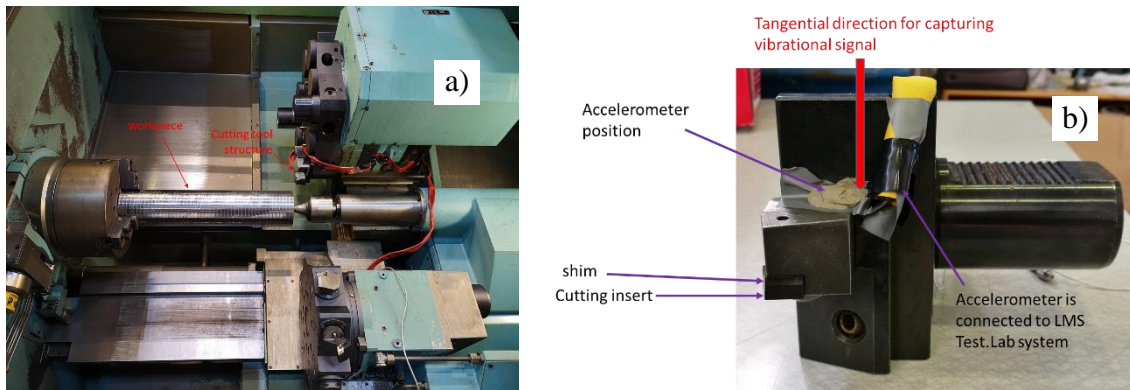

Fig. 6. a) External longitudinal turning operation in SMT-Swedturn-ST300 CNC turning machine;
b) Accelerometer position on cutting tool structure

The cutting insert's flank wear was measured multiple times (in intervals of 16 minutes, 26 minutes and 32 minutes) during the cutting process using Nikon Upright Microscope. The surface roughness value R_a of the machined workpieces was measured with a surface roughness measuring instrument (Mitutoyo Surftest SJ-301) at the end of each machining test (after 32 minutes). Three measuring points were selected along the workpiece bar (the midpoint of the workpiece and both ends). Finishing machining was carried out to generate a better surface finish before measuring the surface roughness. The finishing parameters were cutting speed of 200 mm/min, depth of cut of 1.2 mm, and feed rate of 0.1 mm/rev. The coated shims and their location on the tool holder are illustrated in Fig. 7a and b.
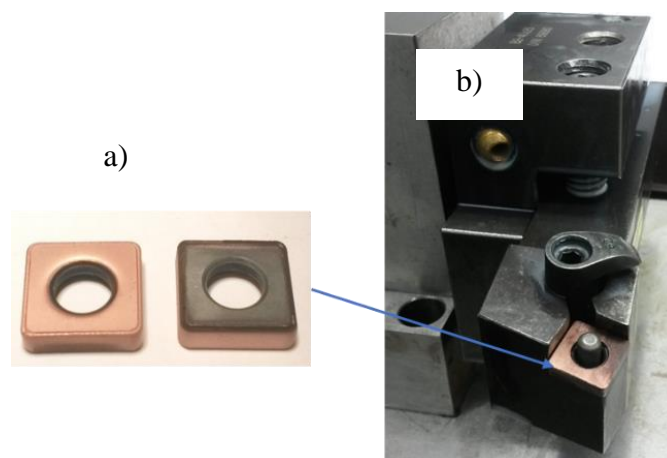

Fig. 7. Cu:CuCNx coated MIRCONA shims (a) used in cutting too structure (b)

5. RESULTS AND DISCUSSION

5.1. CHARACTERISTICS PEAK DISCHARGE CURRENT-VOLTAGE (I-V) WAVEFORM

The detail characteristics of peak discharge current-voltage waveform of reactive-HiPIMS deposition of a-CN$_x$ coating material is described in [22] Form Fig. 8 it can be observed that at the beginning of the pulse in 'ignition phase' though the cathode voltage reaches to its peak value instantly (–750 V), the plasma ignition is delayed by 10 to 12 μs. This 10 to 12 μs of 'glow discharge' can be characterized as comprising of energetic metastable Ar gas atoms.

At 'current rise' phase pulse discharge current reaches to the peak value (–130 A) over the pulse duration while the peak cathode voltage drops from –750 V to –700 V and then at the end of the pulse in 'gas rarefaction' phase the discharge current drops from 130 A to 60 A. During 'current rise' phase N$_2$ and C$_2$H$_2$ precursors as well as Cu atoms become ionized and high-density plasma is created. At 'gas rarefaction' phase the reactive precursors are strongly reduced near the target vicinity.
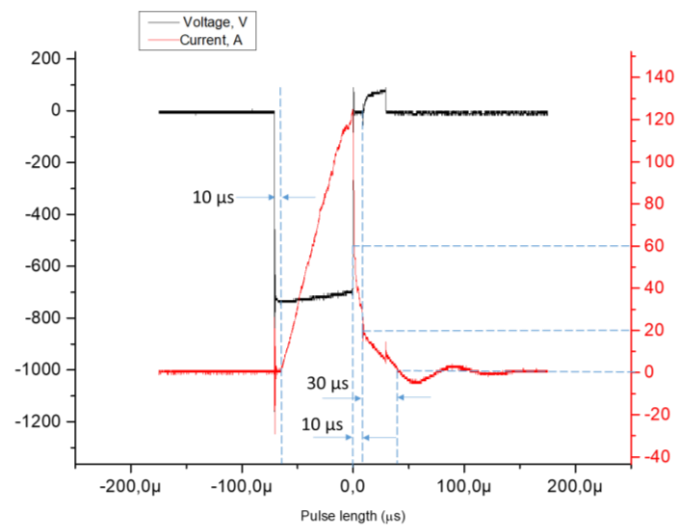

Fig. 8. Cathode Peak voltage and current waveform of HiPIMS of copper target discharge
in reactive Ar/N2/C2H2 environment. Process pressure 0.71 Pa, pulse length 70 μs, pulse frequency 150 Hz

At the end of the pulse within 10 μs the discharge current further drops from 60 A to 20 A, and at this discharge plateau 'self-sputtering' of target ions take place near the target vicinity due to the increase of secondary electron emission. After the end of the pulse at 'after-glow' phase discharge current finally drops from 20 A to 0 A within 30 μs, which indicate the termination of pulse discharge. At this stage low energy ion bombardment of substrate surface takes place. After the termination of the pulse discharge within the duration of 'after-glow' phase, a positive 100 V discharge voltage was applied to the cathode for 20 μs with 10 μs delay. This positive reverse voltage pulse to the cathode is reported to increase the energetic ion flux density near the substrate surface [23].

5.2. MATERIAL AND MECHANICAL CHARACTERIZATION

SEM cross-section image (Fig. 9) of the composite material confirmed the multilayer microstructure of the coating comprising of copper and copper mixed carbon nitride (CN_x-Cu) alternative layers of different thickness. High peak power density and reduced plateau discharge created high ion flux density to the substrates, which facilitated the growth of dense microstructure confirmed by SEM micrograph of the cross section. Unlike the columnar microstructure of a-CN_x reported in [9] neither columnar nor any definite crystal structure of Cu included CN_x phase was found. No cracks or high porosity in the dense microstructure was observed due to high energetic ion bombardment to the substrate surfaces.
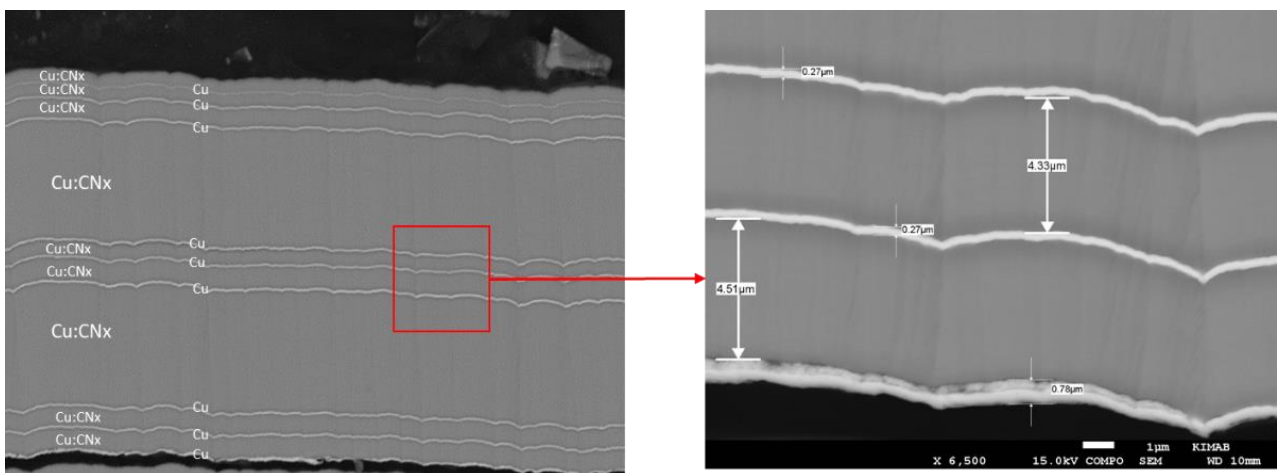

Fig. 9. SEM cross section of Cu:CuCN$_x$ composte coating material (200 μm) showing different Cu and CuCN$_x$ layer

Density of the Cu:CuCN$_x$ multilayer nano-composite coating layer was found to be 3.5 ± 0.05 g/cm^3 (calculated). The total thickness of the coating material was found to be 200 ± 0.1 μm within which 13 thin copper interlayering along with 4 thick CN_x-Cu layers and 10 thin CN_x-Cu layers were observed. Each Cu layer thickness, measured in SEM cross section image, was found to be approximately 0.26 ± 0.06 μm as well as each thick and thin CN_x-Cu layer was 25 ± 0.6 μm and 4.19 ± 0.9 μm respectively.

EDS elemental composition analysis of the cross section reveals that CN_x-Cu phase of the composite coating comprises of approximately 68% Cu, 25% C, 5% N and 1% O (by mass) whereas the thin Cu interlayer incorporates mainly ~82% Cu, 16% C, 2% N and 1% O (by mass). It is worth noting that a little bit of oxygen is always present in different layers of the coating which can be due to the long exposure of coating material in atmospheric environment after deposition process.

Surface and cross-sectional micro hardness of the composite coating material was found to be 305 ± 20 HV and 261.5 ± 17 HV respectively. The high standard deviation in micro hardness can be explained by the inhomogeneity of the coating due to the multi-layered structure. The coefficient of friction of the coating material was found to be 0.20198 at maximum normal force 13.99 N with 10 mm/min scratch speed and maximum 10 mm scratch length.

5.3. MACHINING TEST RESULTS

5.3.1. POWER SPECTRUM DENSITY (PSD) OF ACCELERATION
FREQUENCY RESPONSE FUNCTION (FRF)

The power spectrum density (PSD) of measured acceleration data in tangential direction during machining process was summarized in Fig. 10. Firstly, frequency response function (FRF), acceleration, were measured in the time domain at each cutting run (the moment from the insert plough into the workpiece to the insert run out of the workpiece) during machining, then transferred to PSD through Fast Fourier Transform (FFT). The power spectrum density graphs in Fig. 10 shows that the vibration energy is mostly concentrated in a high frequency range from 3000 Hz to 16000 Hz for all of the measured machining operations. A number of resonance peaks occur within the frequency range from 0 to 25000 Hz. In addition, the maximum peak values in all cutting runs can be observed between 7500 Hz and 8000 Hz. There is no obvious resonant frequency shift, but only distinct peak amplitude reduction was obtained.

This can be explained by the high damping capacity of the 200 μm thick $Cu:CuCN_x$ multilayer nano-composite coating material having a beneficial effect to suppress the high frequency vibrations while retaining the stiffness of the structure. From the frequency band between 7500 Hz to 8000 Hz where the maximum peak occurs, the maximum amplitude of the tool with a conventional shim has a larger range of variation (compared from the beginning to the end of machining, seen from Fig. 10). For the tool with a coated shim, the maximum amplitude increases slightly with the tool wear increase as the machining proceeding. This indicates that a coated shim not only reduce the vibration during machining but also provide a much more stable machining condition. Figure 11 displays the vibration amplitude signals plotted in the time domain for the cutting tool with a conventional shim (red), and the coated shim (green) at cutting run 18 (from 26 minutes to 27 minutes 20 seconds of cutting) in each cutting condition. It is shown that during the machining process, the cutting tool with coated shim has less vibration amplitude which also indicates a more stable cutting process.

From the vibration amplitude measurement in PSD, it can be seen that the damping effect of a coated shim has an apparent influence on cutting tool vibration in the tangential direction. As seen from acceleration measurement in the time domain (Fig. 11), the vibration amplitude of cutting tool with a coated shim is 22% less than the one with a conventional shim. From the power spectrum density graph in Fig. 10, the vibration amplitude with a coated shim was reduced 30%–50% throughout the frequency band. The result demonstrates that $Cu:CuCN_x$ multilayered composite coating improved the damping capacity of cutting tool under practical machining conditions. The similar improvement was also realized by Vladimir A. Rogov et al [24] They observed that a shim made of epoxy granite material, the magnitude value of FRF was adequately reduced compared with a standard shim.

The average surface roughness of the machined workpiece after 32 minutes of turning operation was found to be 0.89 ± 0.07 μm and 0.86 ± 0.07 μm in case of conventional and coated shims respectively.

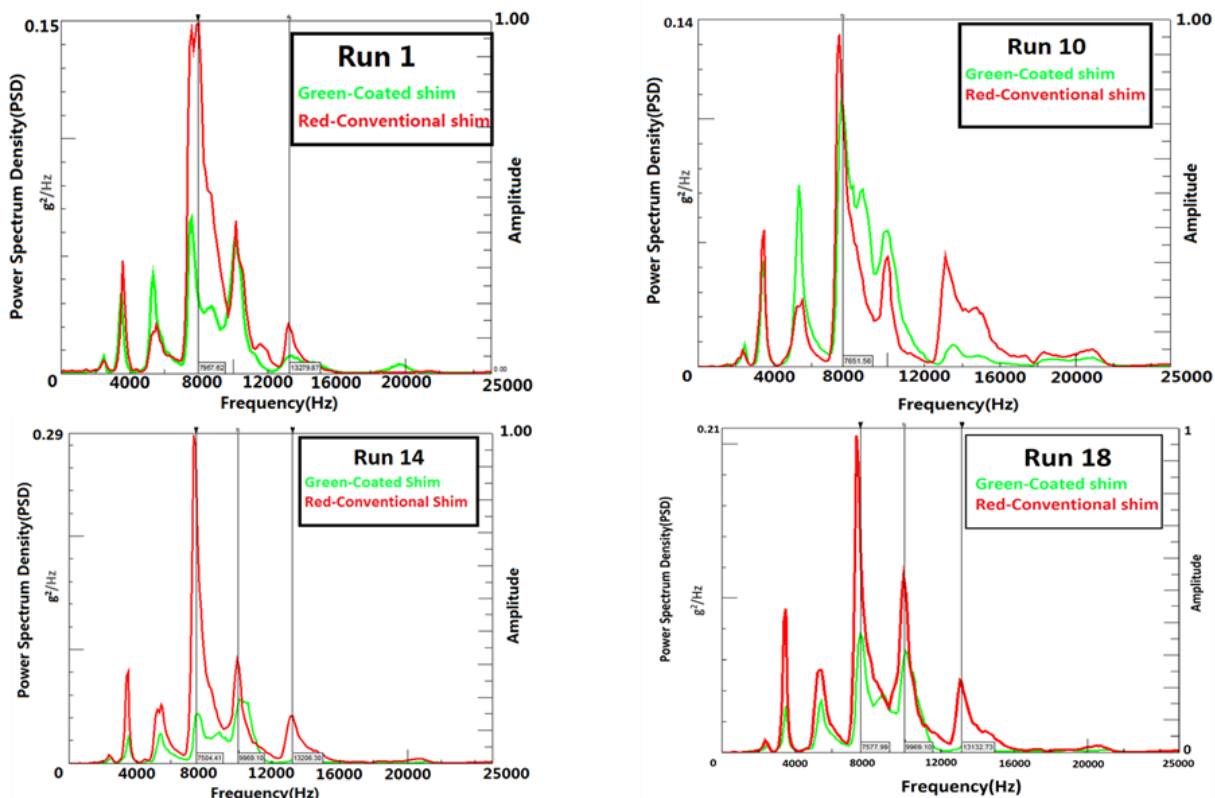Fig. 10. The comparison of power spectrum density of measured acceleration data in the tangential direction of cutting;
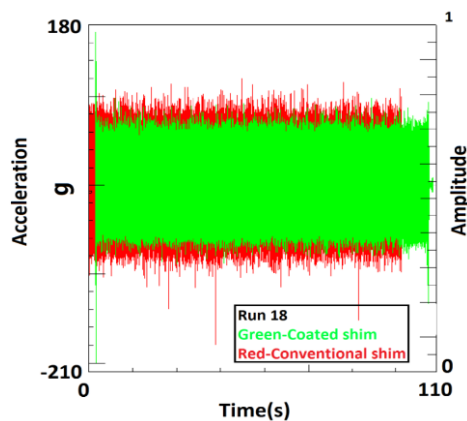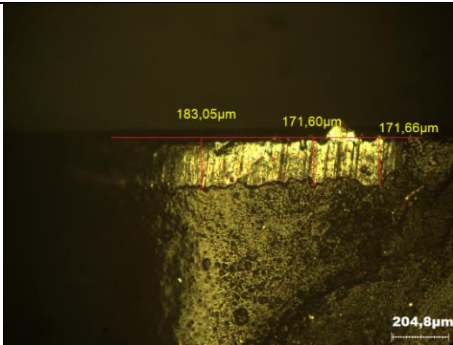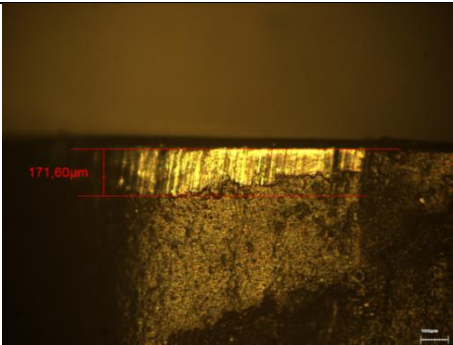run_1: 0 to 2 mins; run_10:15 to 16 mins; run_14: 20 to 21 mins; run_18: 26 to 27 mins
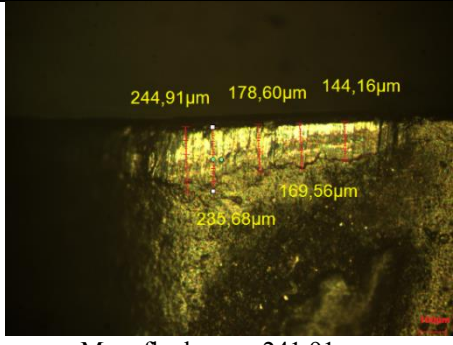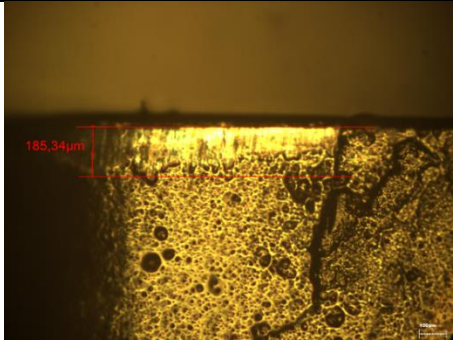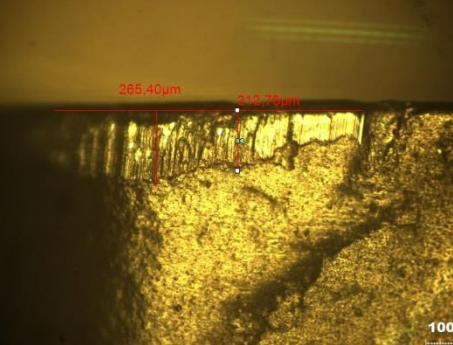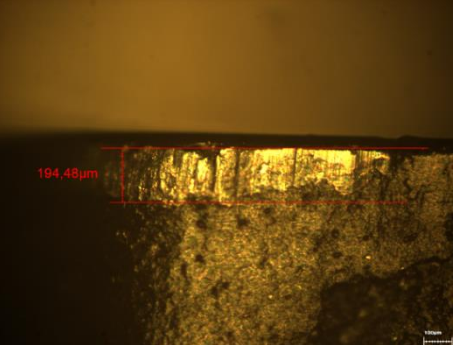

Fig. 11. Comparison of measured acceleration data (in the tangential direction) in time domain
from 26 to 27 mins of cutting

5.3.2. CUTTING TOOL INSERT LIFE EVALUATION

Results of flank wear measurement in each test has been summarized in Table 2. The flank wear was measured in intervals 16 minutes, 26 minutes and 32 minutes. It is apparent that after 32 minutes of machining, the flank wear of the cutting insert with damping coated

shim is minimal which is only 194.48 µm. From 16 minutes to 32 minutes, flank wear increased slightly with a coated shim. On the other side, flank wear with conventional shim reached 265.40 µm after 32 minutes, which is close to the end of tool life (maximum flank wear of 300 µm) according to ISO 3685 standard. Comparing to conventional uncoated shim After 16, 26 and 32 minutes of machining time the maximum insert flank wear were reduced by approximately 6%, 24% and 27% in case of Cu:CuCN$_x$ coated shim.

Table 2. Maximum insert flank wear for conventional and Cu:CuCN$_x$ coated shims

Machining time	Too wear for Conventional shim	Tool wear for Cu:CuCN$_x$ coated shim
16 minutes	Max. flank wear 183.05 µm	Max. flank wear 171.60 µm
26 minutes	Max. flank wear 241.91 µm	Max. flank wear 185.34 µm
32 minutes	Max. flank wear 265.40 µm	Max. flank wear 194.48 µm

The high frequency vibrations on tool tip are caused by the forces applied to the cutting tool during machining and the force originates from the chip formation process. The vibratory energy acted on cutting insert could lead to the deboning of neighboring particles of the insert

which results in the loss of small particles (tool wear). The existence of damping coating under the cutting insert could effectively absorb vibratory energy and dissipate it into other forms of energy (mostly heat). Amir Abdulllah & Mohammad R. Shabgard [25] found that ultrasonic vibration (25 000 Hz) of the tool was more effective in attaining a high material removal rate when machining with cemented tungsten carbide. This explains the high frequency aggressive energy can separate tungsten carbide grains, which have lost the neighboring binder. In our test, the cutting insert was made of tungsten carbide. According to them [25], the high frequency vibrations could accelerate the loss of the tungsten carbide insert particles during machining leading to a fast tool wear. From the measured vibration signal (Fig. 10), it can be clearly observed that on the frequency band from 18 000 Hz to 25 000 Hz, the vibration amplitude with a $Cu:CuCN_x$ coated shim is lower than a conventional shim. Even though the relative amplitude at that frequency range is much lower than the amplitude in low frequency range, but the high frequency micro vibration acted on cutting insert is extremely detrimental to tool life.

6. CONCLUSIONS

Mechanical and physical characteristics of a multilayer nano-composite damping coating are studied in this paper. The coating material is applied on a shim placed beneath the cutting insert. By this, the damping mechanisms is close to the source of vibration. Apart from high damping capacity, the coating material needs to have high stiffness and thermal resistance. The amorphous CN_x coating material was synthesized by means of plasma-enhanced chemical vapor deposition process. For this purpose, high-power impulse magnetron sputtering of Cu target plates was used in reactive $Ar/N_2/C_2H_2$ environment. The mechanical and physical characteristics of the coating material have been analysed in laboratory. Mechanical damping measurement test demonstrated that the deposited CN_x material has damping loss factor value of 0.015 ± 0.001 at high excitation force under first bending deformation mode. From analysis, it was speculated that at high excitation force level interfacial frictional energy loss between the columnar structures as well as horizontal layering structures is the dominating factor for the enhanced damping capacity. The loss modulus $(0.234 \pm 0.011 \text{ GPa})$ of the coating material is higher than the commercial viscoelastic materials.

The theoretic analysis based on the Reuss model shows that for a coated structure, there exist an optimum thickness of the coating layer h_c that makes the product $E^* \tan \delta$ of the coating system reaches the maximum value.

The experimental study demonstrates a significant increase in the tool life of the cutting insert, up to 200%, as well as in the integrity of the machined surfaces.

REFERENCES

[1]   ARCHAMBEAU S., 2004, *What is Your Company's Cost of Poor Quality? Quality Digest*, August. https://www.qualitydigest.com/inside/quality-insider-article/what-your-companyrsquos-cost-poor-quality.html.
[2]   CHUNG D.D.L., 2001, *Review Materials for vibration damping*, Journal of Materials Science, 36, 5733–5737.

[3]   SANDVIK COROMANT, 2017, Silent Tools™ – Damped Tools From Sandvik Coromant, https://www. fgalves.com/wp-content/uploads/2018/03/silent-tools.pdf.

[4]   AMADORI S., CATANIA G., CASAGRANDE A., 2018, *Experimental Evaluation and Modeling of the Damping Properties of Multi-Layer Coated Composites*, Coatings, 8, 53; doi:10.3390/coaTINGS8020053, 1–20.

[5]   GRZESIK W., 2017, *Tribology of Metal Cutting*, Advanced Machining Processes of Metallic Materials, 197–214.

[6]   DAVIM J.P. (ed.), 2012, *Tribology in Manufacturing,* Springer.

[7]   RIVIN E., 2019., *Stiffness and Damping in Mechanical Design,* CRC Press.

[8]   LAZAN B.J., 1960., *Material and Structural Damping for Vibration Control*, SAE Transactions, 68, 537–547.

[9]   HILDEBRAND M., 2005, *Vibration Damping, in Adhesive Bonding, Science, Technology and Applications*, ed. by R.T. Adams, Woodhead Publishing Series, 240–253.

[10]   JOHNSON C.D., 1995, *Design of Passive Damping Systems,* Trans. ASME, June, 117/B, 494–499.

[11]   PRUCZ J.C., KOKKINOS F., SPYRAKOS C.C., 1988, *Advanced Joining Concepts For Passive Vibration Control*, Journal of Aerospace Engineering, 1/4, 193–204.

[12]   TORVIK P.J., 1980, *The analysis and design of constrained layer damping treatments*, *Damping applications fo*r *vibration control*, P.J. Torvik, ed., ASME/Applied Mechanics Division, New York, N.Y., AMD, 38, 851–12.

[13]   FERRY J.D., FITZGERALD E.R., GRANDIENE L.O., 1952, *Temperature-Dependence of Dynimic Proprieties of EIastomers: Relaxation Distribution*, Ind. Eng. Chem., 44/4, 703–706.

[14]   UNGAR E., ZAPFE J.A., 2006, *Structural Damping, in Noise and vibration Control Engineering,* edit by Istvan L. Vér and Leo L., Berenek, John Wiley and Sons, *Technology, Materials Forming, Machining and Tribology*, Springer-Verlag Berlin Heidelberg.

[15]   KOUZNETSOV V., NICOLESCU M., HJALMARSSON Å., KOUZNETSOV K., 2010, *Inventors; Plasmatrix Materials AB*, Stockholm, assignee. Plasma Activated Chemical Vapor Deposition Method and Apparatus Therefor patent US 2011/0081477 A1.

[16]   KOUZNETSOV V., NICOLESCU CM., MEZA O., HEMMINGSSON L., 2008, *Inventors; Plasmatrix Materials* AB, Stockholm, assignee. Method, Material and Apparatus for Enhancing Dynamic Stiffness patent WO2008105736 A3.

[17]   GUDMUNDSSON J., BRENNING N., LUNDIN D., HELMERSSON U., 2012, *High power impulse magnetron sputtering discharge*, J. Vac. Sci. Technol. A 30, 3, 030801.

[18]   KOUZNETSOV V., MACÁK K., SCHNEIDER J.M., HELMERSSON U., PETROV I., 1999, *A novel pulsed magnetron sputter technique utilizing very high target power densities*, Surf. Coat. Technol., 122/2, 290–293.

[19]   KONSTANTINIDIS S., DAUCHOT J.P., GANCIU M., HECQ M., 2006, *Transport of ionized metal atoms in high-power pulsed magnetron discharges assisted by inductively coupled plasm*a, Appl. Phys. Lett. 88, 021501 https://doi.org/10.1063/1.2162671

[20]   VLCEK J., KUDLACEK P., BURCALOVA K., MUSIL J., 2014*, Investigation of ionized metal flux in enhanced high-power impulse magnetron sputtering discharg*es, Journal of Applied Physics, 115, 153301; https://doi.org/ 10.1063/1.4871635.

[21]   STRANAK V., CADA M., HUBICKA Z., TICHY M., HIPPLER R., 2010, *Time-resolved investigation of dual high power impulse magnetron sputtering with closed magnetic field during deposition of Ti–Cu thin films*, Journal of Applied Physics, 108, 043305 https://doi.org/10.1063/1.3467001.

[22]   RASHID M., ARCHENTI A., 2018, *Manufacturing and Characterization of a Carbon-Based Amorphous (a-CN$_X$) Coating Material*, A. Nanomanuf. Metrol., 1, 156–170, https://doi.org/10.1007/s41871-018-0014-y.

[23]   BAOHUA W.U., HAEHNLEIN I., SHCHELKANOV I., MCLAIN J., et al, 2018, *Cu films prepared by bipolar pulsed high power impulse magnetron sputtering*, Vacuum, 150, 216–221.

[24]   ROGOV V.A., GHORBANI S., POPIKOV A.N., NIKOLAY I., 2017, *Polushin,Improvement of cutting tool performance during machining process by using different shim*, Archives of Civil and Mechanical, 17/3, 694–710.

[25]   ABDULLAH A., SHABGARD M.R., 2008, *Effect of ultrasonic vibration of tool on electrical discharge machining of cemented tungsten carbide* (WC-Co), Int J Adv Manuf Technol., 38: 1137–1147, https://doi.org/ 10.1007/s00170-007-1168-8.